National University of Science
and Technology POLITEHNICA
of Bucharest

Faculty of
APPLIED SCIENCE

Specialisation
PHYSICS ENGINEERING

Abstract

APPLICATIONS OF IONIZING RADIATION BEAMS FOR IRRADIATIONS IN THE ATMOSPHERE

Student
Alexandru ENCIU

Thesis coordinator
prof. dr. Gheorghe CĂTA-DANIL

Scientific coordinator
cs1 dr. Mihai IOVEA

Bucharest, September 2023

National University of Science
and Technology POLITEHNICA
of Bucharest

Faculty of
APPLIED SCIENCE

Specialisation
PHYSICS ENGINEERING

Abstract

APPLICATIONS OF IONIZING RADIATION BEAMS FOR IRRADIATIONS IN THE ATMOSPHERE

Doctorand
Alexandru ENCIU

Doctoral Committee

Chair	Prof.dr. Cristina STAN	National University of Science and Technology Politehnica of Bucharest, Faculty of Applied Science
Thesis Coordinator	Prof. dr. Gheorghe CĂTA-DANIL	National University of Science and Technology Politehnica of Bucharest, Faculty of Applied Science
Member	Conf. dr. Gabriel SULIMAN	National University of Science and Technology Politehnica of Bucharest, Faculty of Applied Science
Member	Prof. dr. Mihaela SIN	University of Bucharest, Faculty of Physics
Member	CSII. dr. Gihan VELIȘA	Horia Hulubei National Institute for R&D in Physics and Nuclear Engineering

Contents

Chapter 1

Introduction

This thesis was conducted at the 3 MV accelerator of the Horia Hulubei Institute of Physics and Nuclear Engineering (IFIN-HH) in collaboration with the company Sc. AccentPro2000 SRL. It focuses on the development of equipment and methods for three research directions. The first research topic focuses on the development of a elemental mapping system for geological samples based on X-ray Fluorescence (XRF). This system was developed as a platform for the other two topics addressed in this work. The second and third topics are based on the development of a proton beam irradiation system in air, which was used for elemental mapping of samples using Particle Induced X-ray Emission (PIXE) and the pulsed irradiation of in vitro biological samples. The results obtained have been the subject of three AIS-rated publications.

The thesis manuscript is structured into five chapters. The first chapter provides an introduction to the field and the methodology. The second chapter presents the theoretical considerations of X-rays and accelerated proton beams. Chapters 3 and 4 cover the development of equipment and methods for the mentioned topics, with Chapter 5 summarizing the general conclusions and perspectives on the presented topics.

In Chapter 1, a brief history of ionizing radiation applications is presented, starting from their discovery by W. C. Roentgen and H. Becquerel in 1895-1896, up to the most recent developments in the field. The moti-

vations for the chosen research topics are also briefly outlined.

Chapter 2

X-rays and Proton Beams

In the first part of Chapter 2, the theoretical considerations necessary to understand the physical phenomena that occur during the interaction of X-rays and proton beams with matter are addressed. The production of X-rays is explained, including the two main production mechanisms: bremsstrahlung X-rays resulting from the deceleration of electrons in the electric field of atoms and characteristic X-rays originating from radiative electron transitions between atomic orbitals (Figure 2.1).

This chapter also covers the operation of X-ray generators, as they are the primary source of X-rays used in applications. To understand their operation, the "SpeckCalc" software was used to simulate the X-ray emission spectrum for various operating parameters, such as the variation of beam current and acceleration voltage (Figure 2.2b and 2.2a).

Since two of the research topics in the thesis are based on X-ray spectroscopy, the section dedicated to the electronic structure of atomic layers provides the necessary theory to understand the structure of atomic orbitals and the mechanisms of electron transitions between them, as dictated by quantum mechanics (Figure 2.3).

The section on X-ray interaction with matter describes the mechanisms illustrated in Figure 2.4. These phenomena contribute to both the attenuation of the primary beam and the attenuation of characteristic X-rays emitted during elemental analysis. The law that describes attenuation is

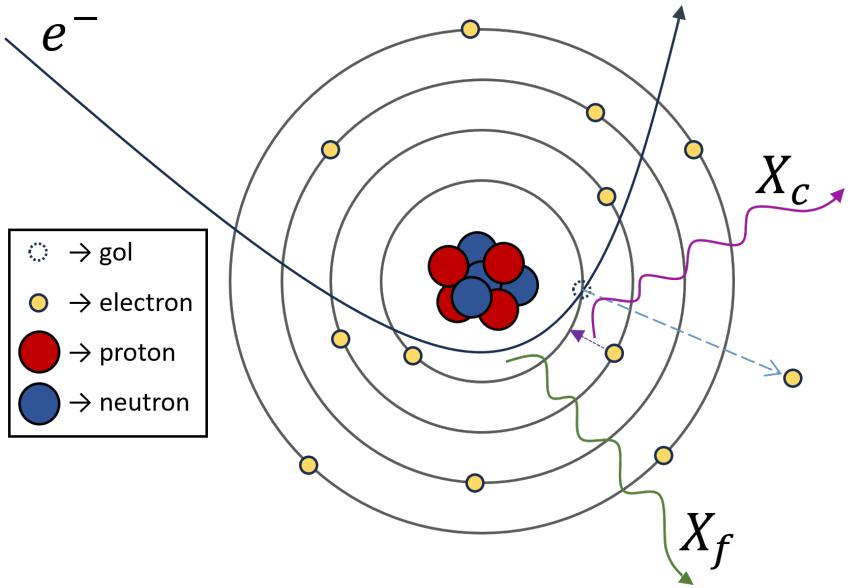

Figure 2.1: The graphical representation of the two mechanisms for producing X-rays following the excitation of an atom by accelerated electrons, where e^- represents the incident electron, and X_f and X_c are the bremsstrahlung and characteristic X-rays, respectively.

exponential and is known as the Beer-Lambert law.

In the second part of Chapter 2, the production of proton beams from gaseous targets using ion sources such as the plasmatron and from solid targets using sputtering sources is discussed. Additionally, the interaction of proton beams with matter is studied by comparing two simulations of energy loss per unit length for a 3 MeV proton beam and a 15 keV X-ray beam. This comparison highlights the exponential nature of X-rays in contrast to the Bragg peak curve for protons, where the highest energy loss occurs at the Bragg peak (Figure 2.5).

Two of the thesis research topics focus on qualitative and quantitative elemental analysis. In the final part of Chapter 2, elemental analysis with X-rays and proton beams is discussed, emphasizing the linear dependence between X-ray intensity and mass fraction for thin samples and the non-linear behavior in thick samples due to the self-absorption effects of X-rays

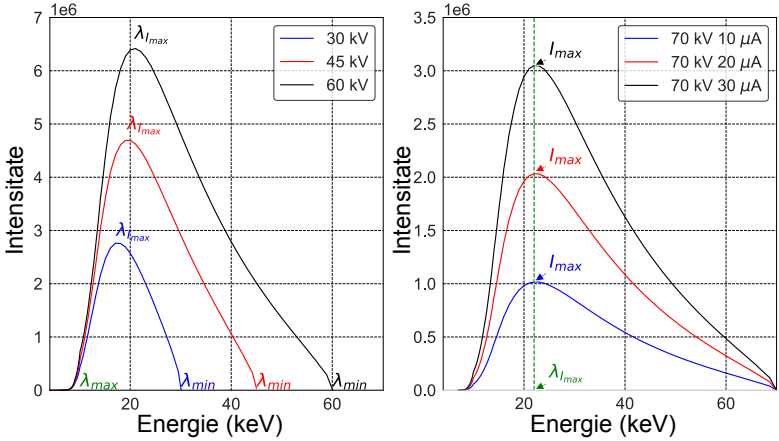

(a) (b)

Figure 2.2: a. Simulating the continuous spectrum using "SpekCalc" for electron beam acceleration voltages of 30, 45, and 60 kV to highlight the variation of $\lambda_{I_{max}}$ as a function of the incident energy of the electron beam. b. Simulating the continuous spectrum for an acceleration voltage of 70 kV and beam currents of 10, 20, 30 μA to emphasize the variation of the amplitude I_{max} as a function of the number of electrons interacting with the target per unit of time.

in the sample. The influences of secondary X-ray emission on elemental concentration calculations are also addressed.

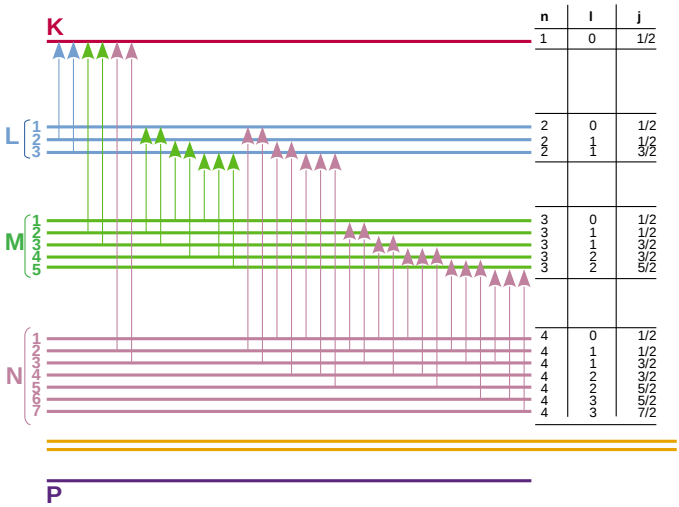

Figure 2.3: The allowed electron transitions between the K, L, M, and N shells.

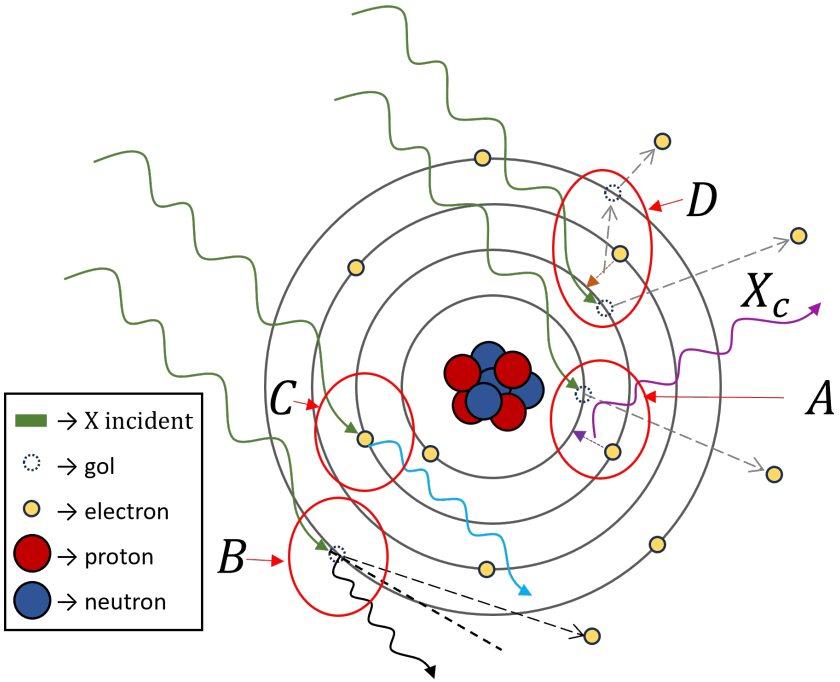

Figure 2.4: Graphic representation of: A. Photoelectric Effect; B. Compton Effect; C. Rayleigh Scattering; D. Auger Effect.

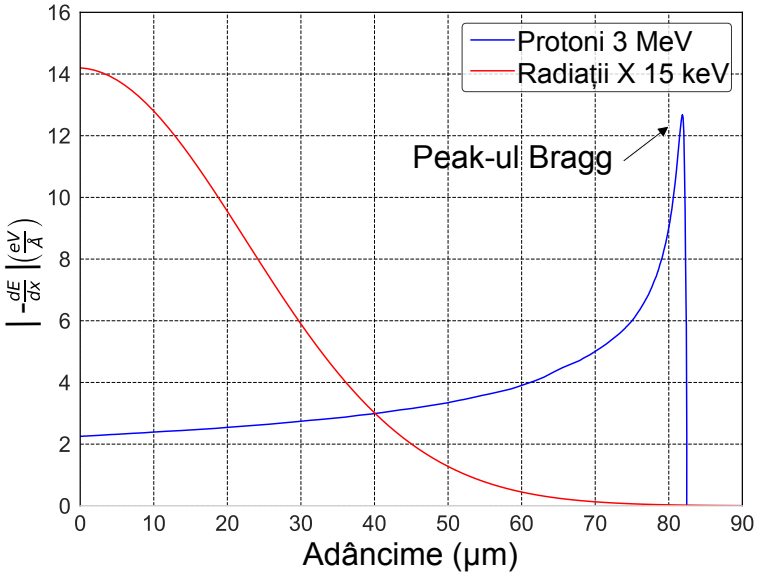

Figure 2.5: Comparison between the energy deposited by a 15 keV X-ray beam and a 3 MeV proton beam when passing through an aluminum target.

Chapter 3

2D/3D Elemental Mapping System for Samples Using XRF

Chapter 3 addresses the development of equipment and methodology for an experimental setup capable of performing 2D and 3D elemental mapping. Initially, this system served as a development and testing platform for the proton beam irradiation system described in Chapter 4. The results obtained during the tests exceeded expectations, leading to the refinement of the system and its use in scanning geological cores without the need for additional processing.

Currently, there are two types of scanners for geological cores. One-dimensional scanners, such as the ITRAX®, scanner produced by Avaatech, can only scan the length of the core, generating a distribution map of elemental concentrations based on the core's length. The main disadvantage of this type of scanner is the additional processing required before scanning, leading to additional costs. The second type of scanner widely used in geology is the M4Tornado®, produced by Bruker. It can produce 2D elemental maps, but like the ITRAX®, the cores must be sectioned to expose a flat surface, limiting the scanned area to a few square centimeters

due to the small size of the device.

This chapter describes an experimental assembly capable of producing elemental mapping on the cylindrical surface of geological cores without the need for additional processing and reconstructing elemental maps in 1D, 2D, and 3D visualization modes.

The experimental assembly (Figure 3.1) consists of a dedicated sample manipulator that allows sample movement on two translation axes and one rotation axis, an X-ray generator for X-ray fluorescence, and an X-ray detector for measuring the characteristic X-rays emitted by the sample. The integration of the system is achieved through dedicated control software developed using the LabVIEW programming language. This software enables independent control of the system components and automation of the entire scanning process.

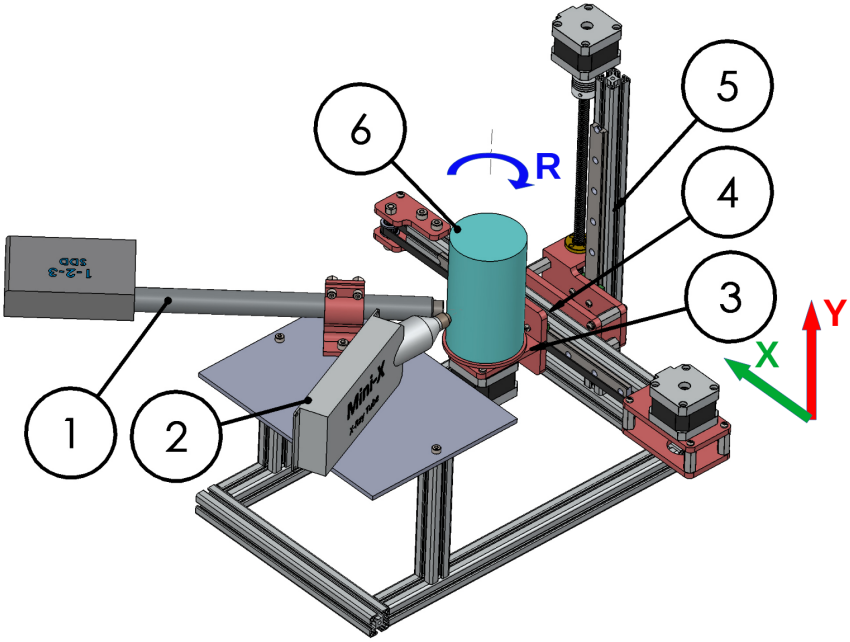

Figure 3.1: CAD project of the experimental assembly: 1. X-ray radiation detector; 2. X-ray radiation generator; 3. Rotating table R; 4. X-axis translation; 5. Y-axis translation; 6. Analyzed sample.

The reconstruction of elemental maps involves the precise extraction of

X-ray intensity values measured for each measurement point. These values can be extracted after performing a fitting and additional corrections for detection efficiency and X-ray production probability.

The commissioning of the entire system was performed using a breccia sample. The data obtained was used to develop and refine the reconstruction and visualization algorithms for 1D (Figure 3.2), 2D (Figure 3.3) and 3D (Figure 3.4b) modes. In 1D mode, the measured spectra from a measurement layer are summed, and the X-ray intensity values for each element present are graphically represented as a function of height. In 2D mode, the relative abundance of chemical elements on the unfolded cylindrical surface is represented. The color scale represents the relative quantity of a chemical element for each element at each measurement point. The 3D representation mode allows the localization of mineral conglomerates on the cylindrical surface in a 3D virtual space, where the color of each element indicates the species of atoms located at a measurement point.

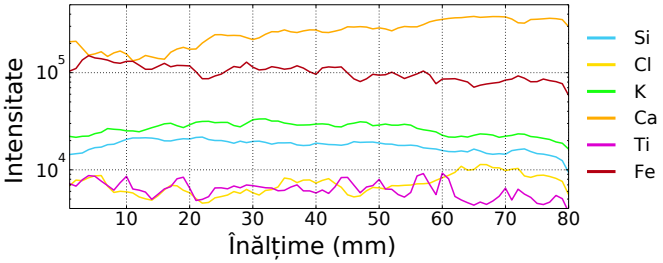

Figure 3.2: 1D Representation: Relative abundance of elements as a function of sample height for the analyzed sample.

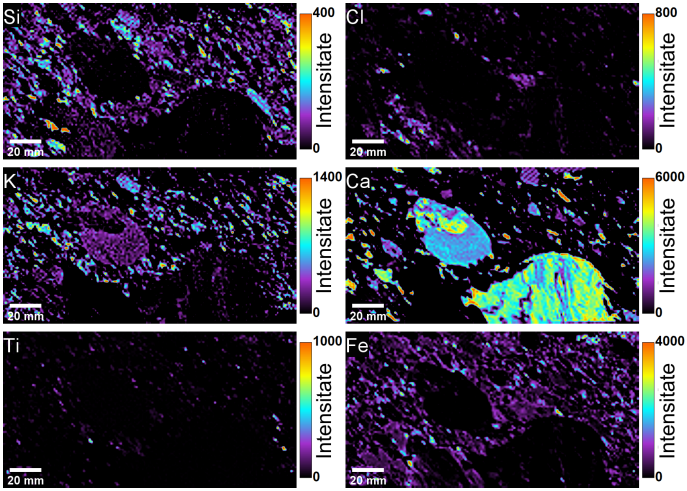

Figure 3.3: 2D Representation: Reconstructed elemental maps for Si, Cl, K, Ca, Ti, and Fe.

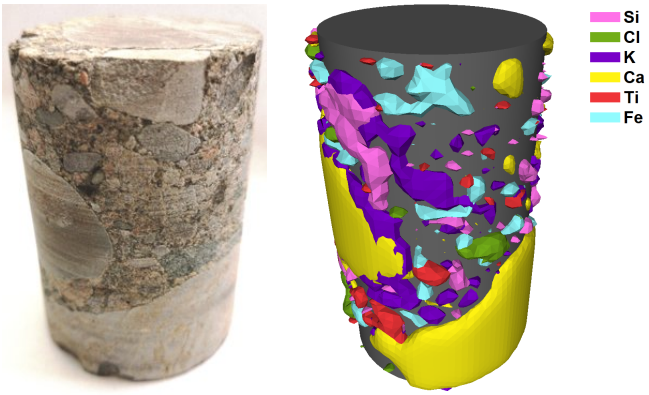

(a) (b)

Figure 3.4: 3D Representation: A. The sample used for commissioning, with a diameter of 60 mm and a height of 80 mm. B. 3D reconstruction for the elements Si, Cl, K, Ca, Ti, and Fe.

Chapter 4

External Proton Beam Irradiation System

Chapter 4 of the thesis addresses the development of hardware, software, and work methodology for an irradiation system installed on the IBA line of the 3 MV IFIN-HH accelerator, which uses a proton beam extracted into the air. The main applications of this system include the irradiation of in vitro biological samples with pulsed proton beams, the determination of elemental concentrations, and 2D elemental mapping using PIXE.

To ensure optimal conditions for the irradiation of biological samples and PIXE analyses, the irradiation system can be used in two configurations referred to as the "Irradiation Configuration" and the "PIXE Configuration" (Figura 4.1). In the configuration for irradiating biological samples (Figura 4.1 A), the proton beam is deflected by an electrostatic deflector controlled by a pulsing unit into one of the accelerator collimators. The beam reaches the target direction only during a pulse. To ensure beam uniformity, a thin gold foil scatters protons, broadening the Gaussian profile of the beam. Extraction of the beam into the air is achieved through a 10x10 mm^2 or 15x15 mm^2 silicon nitride window, depending on the desired irradiation area. Alignment of the sample with the proton beam is achieved using a video camera and two alignment lasers. Sample movement is facilitated by a sample manipulator with X, Y, and Z axes,

which can be controlled remotely.

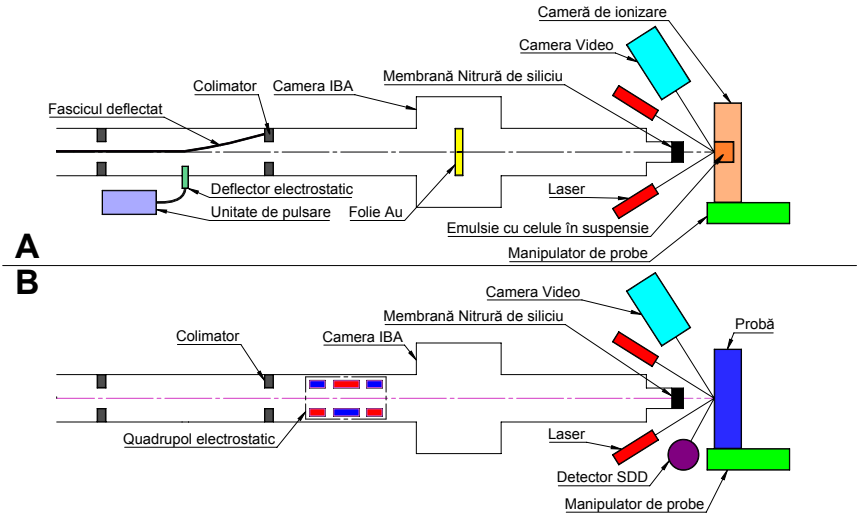

Figure 4.1: Block diagram of the two operating configurations of the external proton beam irradiation system: A. The configuration used for pulsed irradiation of biological samples. B. The configuration used for PIXE analysis.

In the experimental configuration for PIXE elemental analysis (Figura 4.1 B), the proton beam is focused using an electrostatic quadrupole lens located before the IBA reaction chamber, directly onto the sample, through a 3x3 mm^2 silicon nitride window. Similar to irradiation of biological samples, sample alignment is done using two lasers, a video camera, and a sample manipulator. A silicon detector is used to detect the X-rays emitted during PIXE, and helium is injected at a constant flow rate into the space between the sample and the detector to reduce X-ray intensities in the air.

Pulsing of the proton beam for biological sample irradiation is achieved using a pulsing unit controlled by a PC via a signal generator. The block diagram of the operation can be seen in Figure 4.2. Tests (Figure 4.3) have shown that the shape and duration of the proton pulses are in line with the set values. To automate and miniaturize the entire irradiation system, a dedicated circuit was designed and controlled by the control software

developed as part of the thesis.

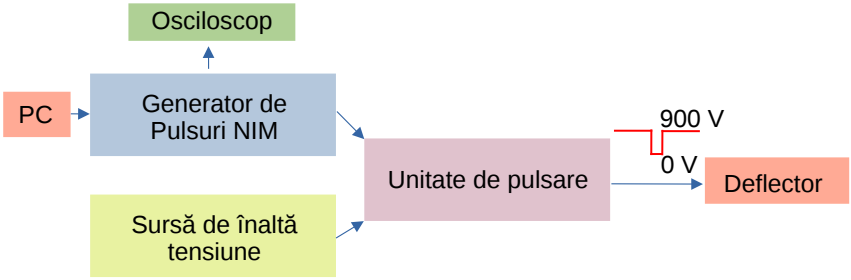

Figure 4.2: Logic diagram of the system that generates pulsed high voltage for the electrostatic deflector.

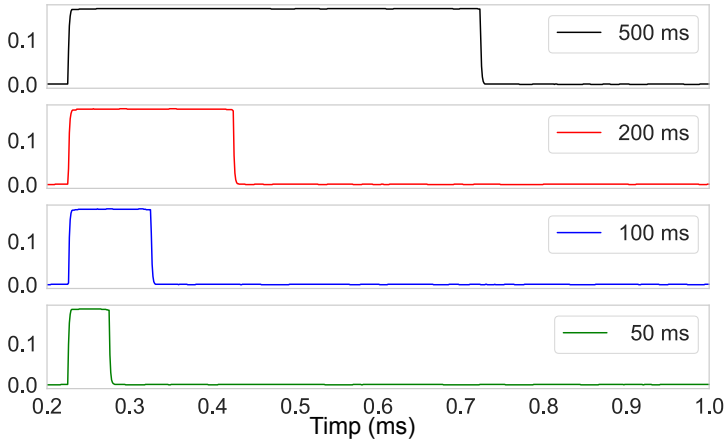

Figure 4.3: Testing the pulsing unit with a proton beam, pulses with durations of 50, 100, 200, 500 ms.

Extraction of the proton beam into the air for the two working configurations is accomplished using three silicon nitride windows, each of which is used depending on the desired irradiated area. In this thesis, a new sealing procedure was developed for the 3x3 mm^2 window to increase its longevity (Figure 4.4). The procedure involves applying a double-sided carbon adhesive film to the mounting support surface, ensuring optimal

thermal contact and even dissipation of mechanical stresses. Vacuum sealing of the window is achieved by applying a dedicated epoxy resin to the window edges.

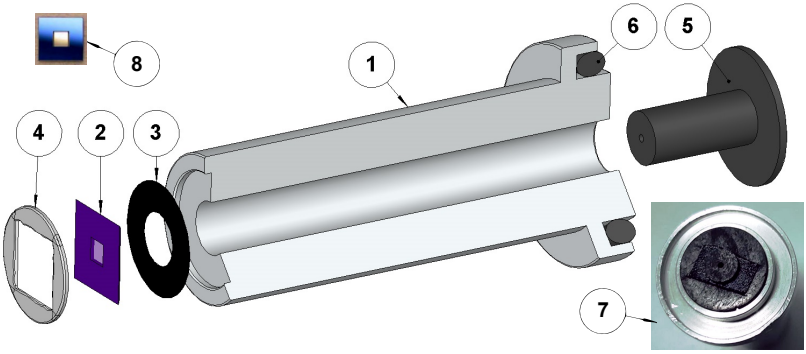

Figure 4.4: CAD drawing of the support for mounting the 3x3 mm Si_3N_4 membrane: 1. Aluminum support; 2. Si3N4 window; 3. Double-sided carbon adhesive tape substrate; 4. Loctite® EA 9492 epoxy resin; 5. Graphite collimator; 6. Rubber seal gasket; 7. Image of the graphite collimator; 8. Image of the Si3N4 window before assembly.

Regarding the 15x15 mm^2 window, it was designed, manufactured, and tested as part of the thesis (Figure 4.5). The CAD drawing of this window can be seen in Figure X. Large-sized windows come pre-mounted on an aluminum support by the manufacturer. This support is placed in an intermediate support that screws onto the accelerator's vacuum column extension. Tests (Figure 4.6) with proton beams on a radiochromic film revealed that the shape and uniformity of the proton beam are consistent with expectations.

Biological samples to be irradiated are grown directly on a mylar foil, which is placed in an irradiation chamber that ensures sterility and hydration. Two versions of irradiation chambers were used in the thesis. The first version was used exclusively for manual irradiations in combination with the 10x10 mm^2 silicon nitride window. The second version (Figure 4.7 and 4.8) of the irradiation chamber, which was designed, fabricated, and tested as part of this work, was used in combination with the 15x15 mm^2

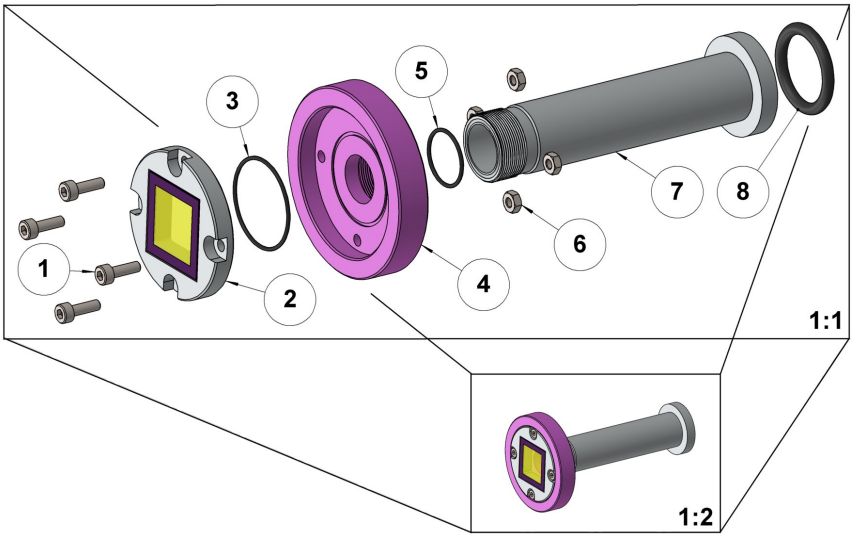

Figure 4.5: CAD drawing of the support for mounting the Si_3N_4 windows of 10x10 and 15x15 mm: 1. M3 screws; 2. Si_3N_4 window mounted on an Al frame; 3. Gasket that ensures sealing between the window frame and the intermediate support; 4. Intermediate support; 5. Gasket that ensures sealing between the intermediate support and the Al extension; 6. M3 nuts; 7. Al extension; 8. Gasket that ensures sealing with the accelerator column.

window. The second version is still undergoing testing and commissioning.

During PIXE analyses, the characteristic X-rays emitted by the sample experience attenuation when passing through the air between the detector and the sample. Therefore, a system was developed in this thesis to blow helium into the space between the detector and the sample during PIXE analyses. In Figure 4.9, a simulation of X-ray transmission through 1.5 cm of air and helium can be seen. The graph shows that X-rays below 2 keV are completely absorbed, while in the case of helium, the loss is only 1.4%. The helium blowing nozzle (Figure 4.10) was 3D printed using PLA plastic. Gas flow simulations (Figure 4.11) for a single nozzle showed that the helium pillow created is unstable, resulting in inefficient displacement of air from that region. To stabilize the helium pillow, helium blowing must occur from at least two directions. To validate the simulations, an experiment

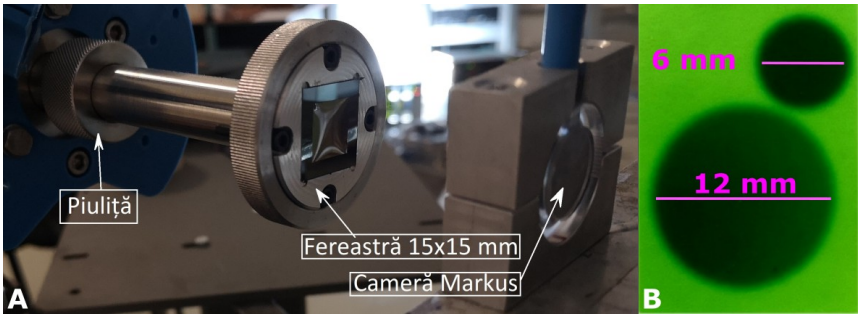

Figure 4.6: A. Testing the 15x15 mm window under vacuum; B. Testing the 10x10 mm and 15x15 mm windows with a proton beam on radiochromic film.

was conducted in which the NIST 611 standard material was measured with PIXE for helium blowing from one direction and two directions at a total flow rate of 3 l/min. The X-ray spectra recorded can be seen in Figure 4.12. Since the helium pillow is much more efficient when helium is blown from two directions, the background radiation is reduced, and the following elements are better highlighted.

The hardware components of the system were integrated by mounting them on 3D printed supports, resulting in reduced design times and costs. In Figure 4.13, the CAD drawing of the system used in the PIXE configuration can be seen. The main support is mounted on the accelerator exit window. The X-ray detectors are positioned at a 35-degree angle and 1.5 cm from the sample. Alignment lasers are located below the X-ray detectors at a 40-degree angle. The camera's location is just below the alignment lasers, mounted on the accelerator column using 3D printed supports. Since all the supports used are 3D printed, the weight of the entire system has been significantly reduced, leading to reduced mechanical stress on the accelerator's vacuum column.

The software integration of the irradiation system was carried out using the LabVIEW programming language. The dedicated software is capable of individually controlling all components of the system (detectors, lasers, probe manipulator, electrostatic deflector) and can also automatically perform irradiation operations in both pulsed mode and elemental mapping.

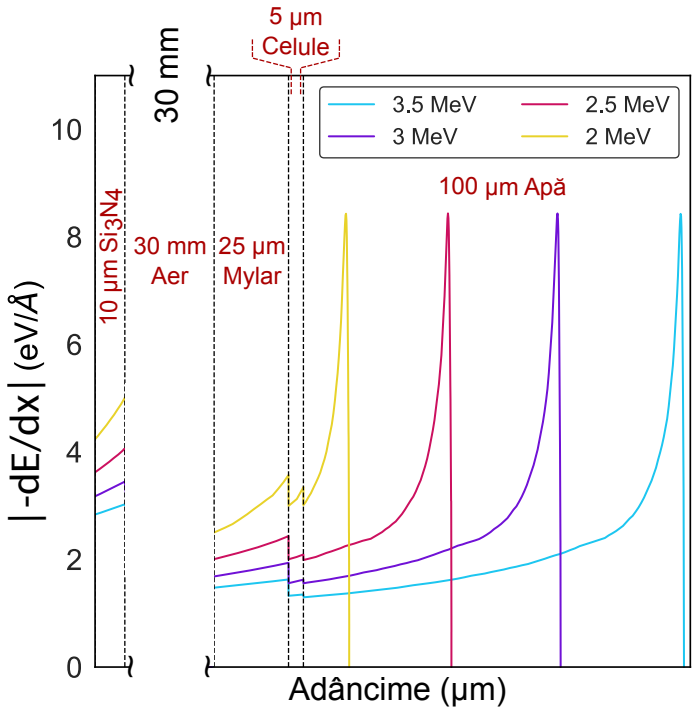

Figure 4.7: Simulation of proton energy loss in irradiation chambers using SRIM-2013.

The commissioning of the external proton beam irradiation system for in vitro biological sample irradiations was performed on fibroblast cell cultures, and their survival rate was measured. The results were consistent with findings published by other laboratories and are the subject of an article with an AIS impact factor.

Regarding the commissioning of the system for elemental analyses, it was tested on a set of 40 archaeological bronze samples to determine elemental concentrations. System calibration was carried out using the BCR-691 A-E bronze standards (Figure 4.14), and the interpretation of the results will be published by the beneficiary.

Elemental mapping of the samples was performed according to the scheme in Figure 4.15. The commissioning of the system was carried out on a set of 3 samples, one archaeological sample and two geological samples.

The variation in proton beam intensity over time was compensated for using a reference plate. The effect of this type of correction can be observed in Figure 4.16. The results obtained from the scanning were satisfactory, and the reconstruction of elemental maps can be visualized in Figures 4.17, 4.18, and 4.19.

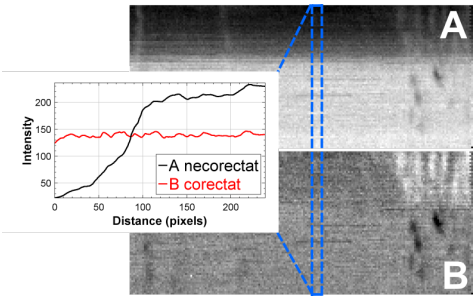

Figure 4.16: Elemental map before (A) and after (B) applying the proton beam intensity variation correction.

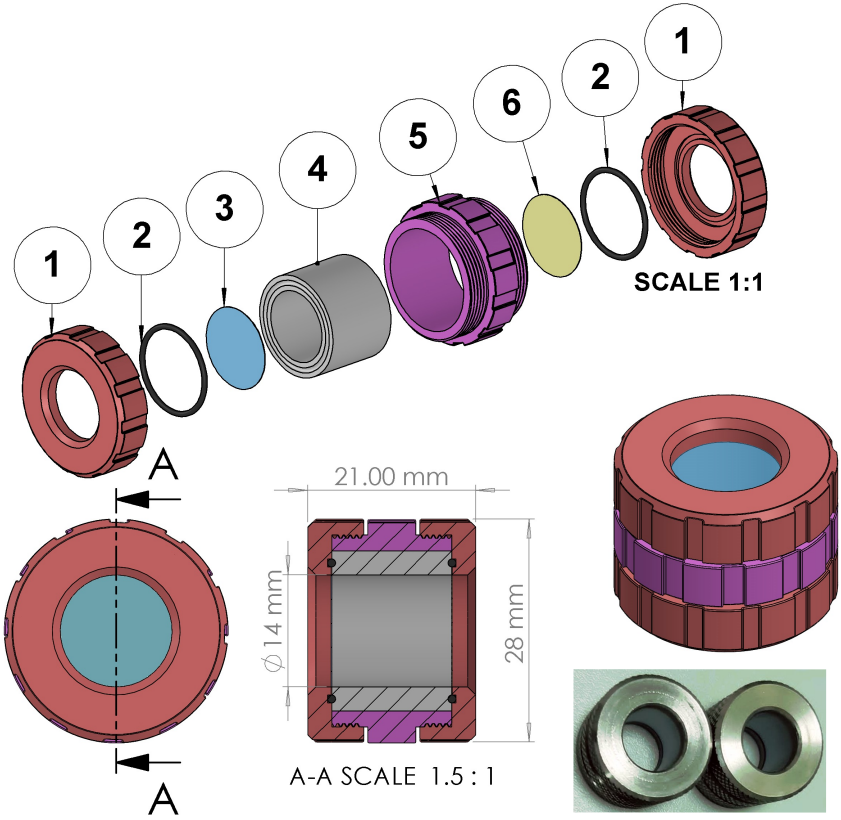

Figure 4.8: CAD drawing of version 2 of the irradiation chamber for biological samples: 1. Threaded cap; 2. Seal gasket; 3. Mylar film; 4. Teflon insert; 5. Casing; 6. Sterile membrane for cell respiration.

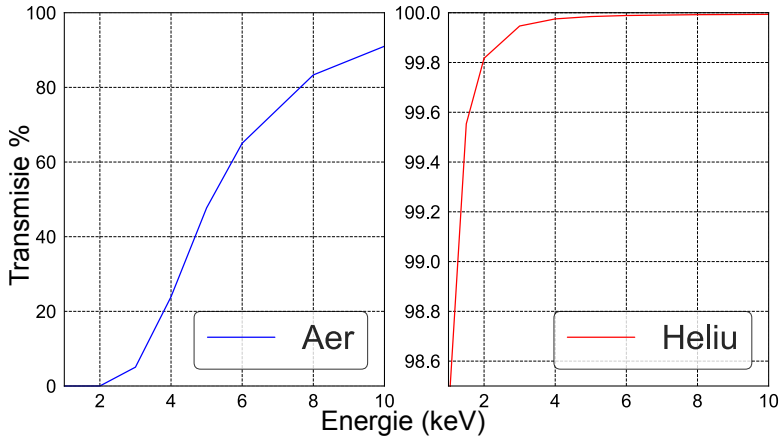

Figure 4.9: Comparison of X-ray transmission through air and through helium over a distance of 1.5 cm.

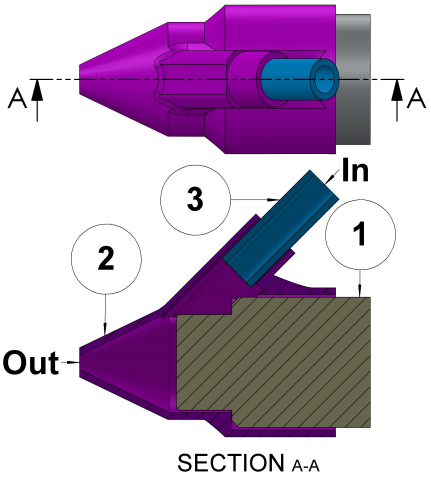

Figure 4.10: CAD diagram of the nozzle applied to the X-ray radiation detector to inject helium into the space between the detector and the sample. 1. X-ray radiation detector; 2. Helium nozzle; 3. Hose transporting helium to the nozzle

;

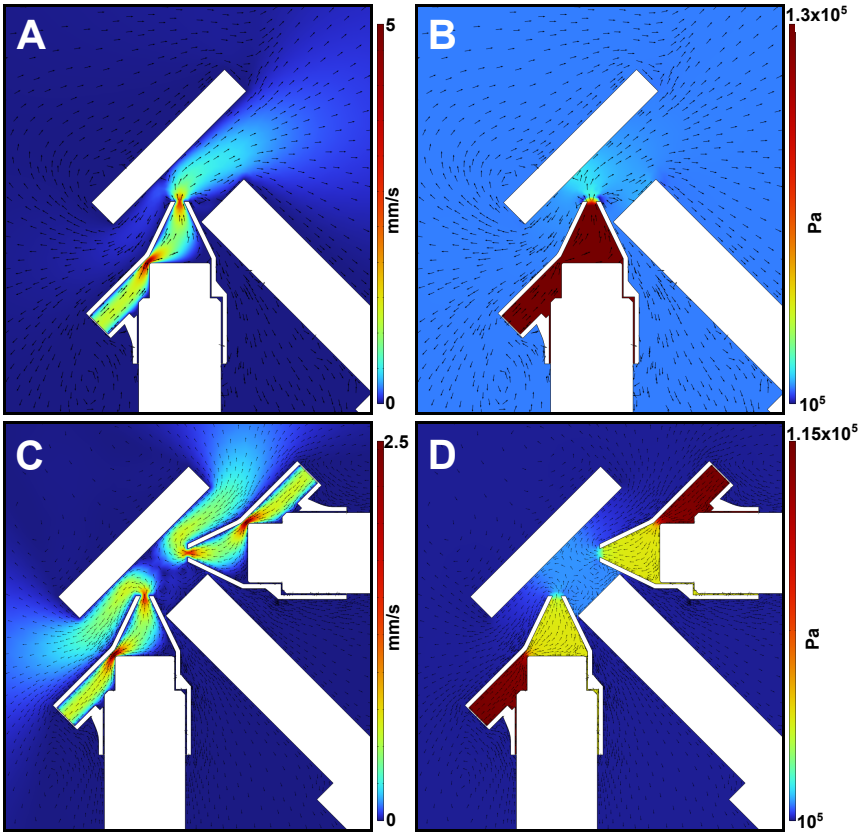

Figure 4.11: A, C. Simulation of laminar helium flow in COMSOL Multiphysics for a single nozzle and two nozzles. B, D. Simulation in COMSOL Multiphysics of the helium cushion created for a single nozzle and two nozzles.

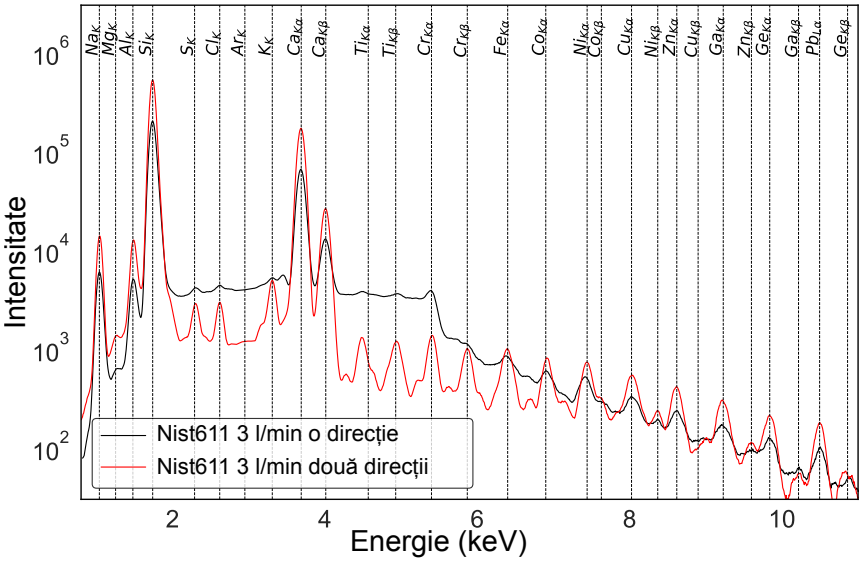

Figure 4.12: Comparison between the spectra of the NIST-611 standard material when exposed to helium flow from one direction and two directions at a flow rate of 3 l/min of helium.

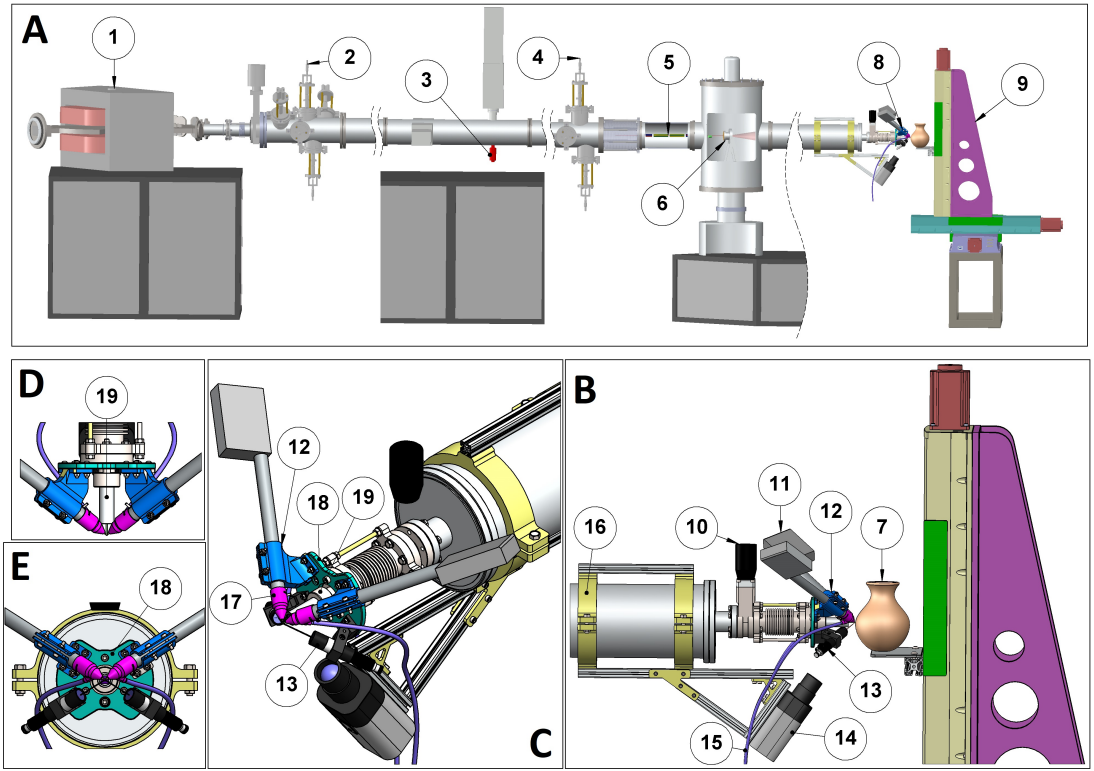

Figure 4.13: A. The IBA line with the proton irradiation system in air; Proton irradiation system; B. Side view; C. Front-right view; D. Top view; E. Front view; 1. Magnet; 2,4. Collimators; 3. Electrostatic deflector; 5. Electrostatic Q-pol; 6. Au foil; 7. Sample; 8. Air irradiation system; 9. Sample manipulator; 10. Chamber; 11. SDD Detector; 12. Detector support; 13. Laser; 14. Camera; 15. Helium hose; 16. Camera clamping rings; 17. Helium nozzle; 18. Mounting bracket; 19. Si_3N_4 window.

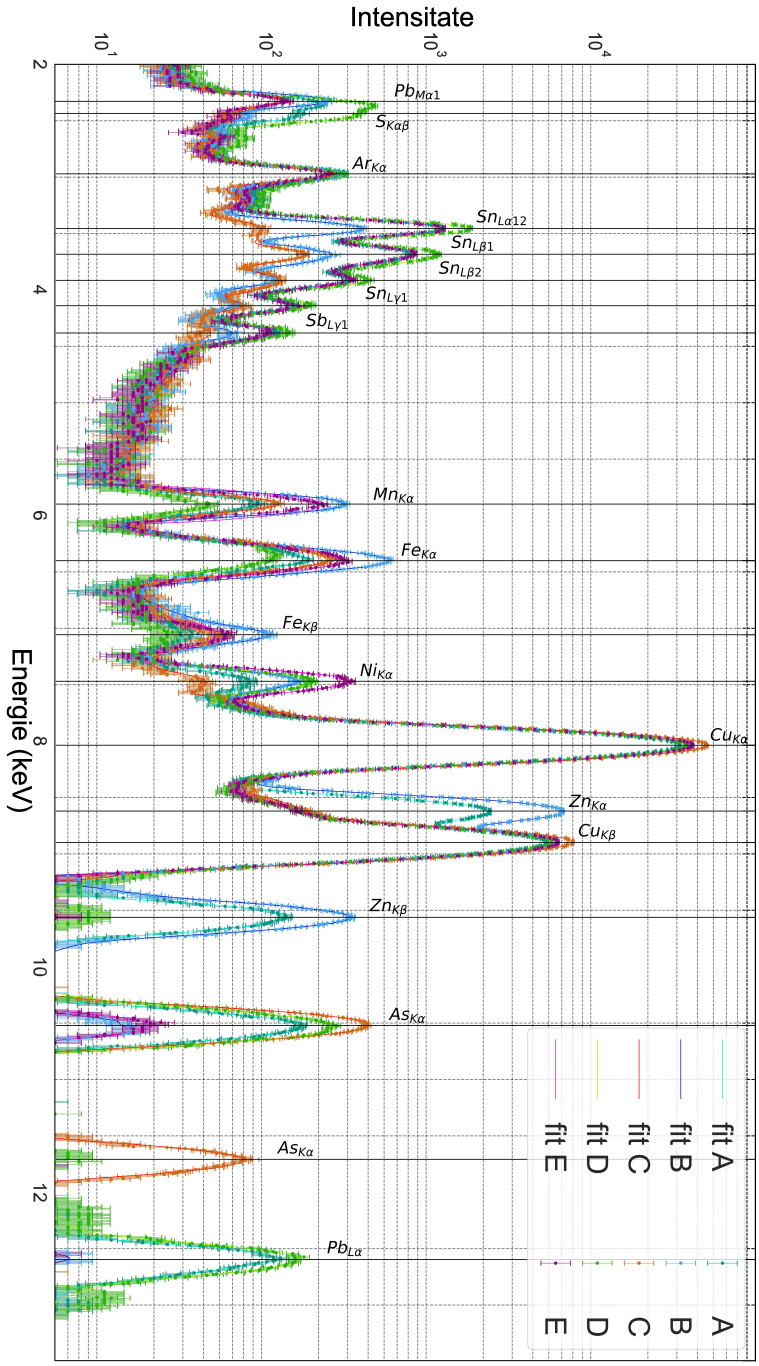

Figure 4.14: The X-ray spectrum emitted as a result of PIXE for the bronze standards A, B, C, D, and E of BCR-691.

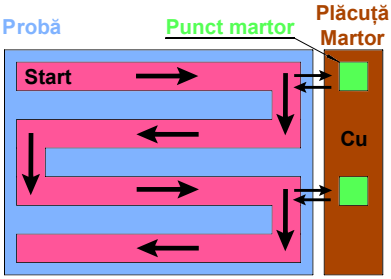

Figure 4.15: Graphic representation of the elemental mapping process using PIXE.

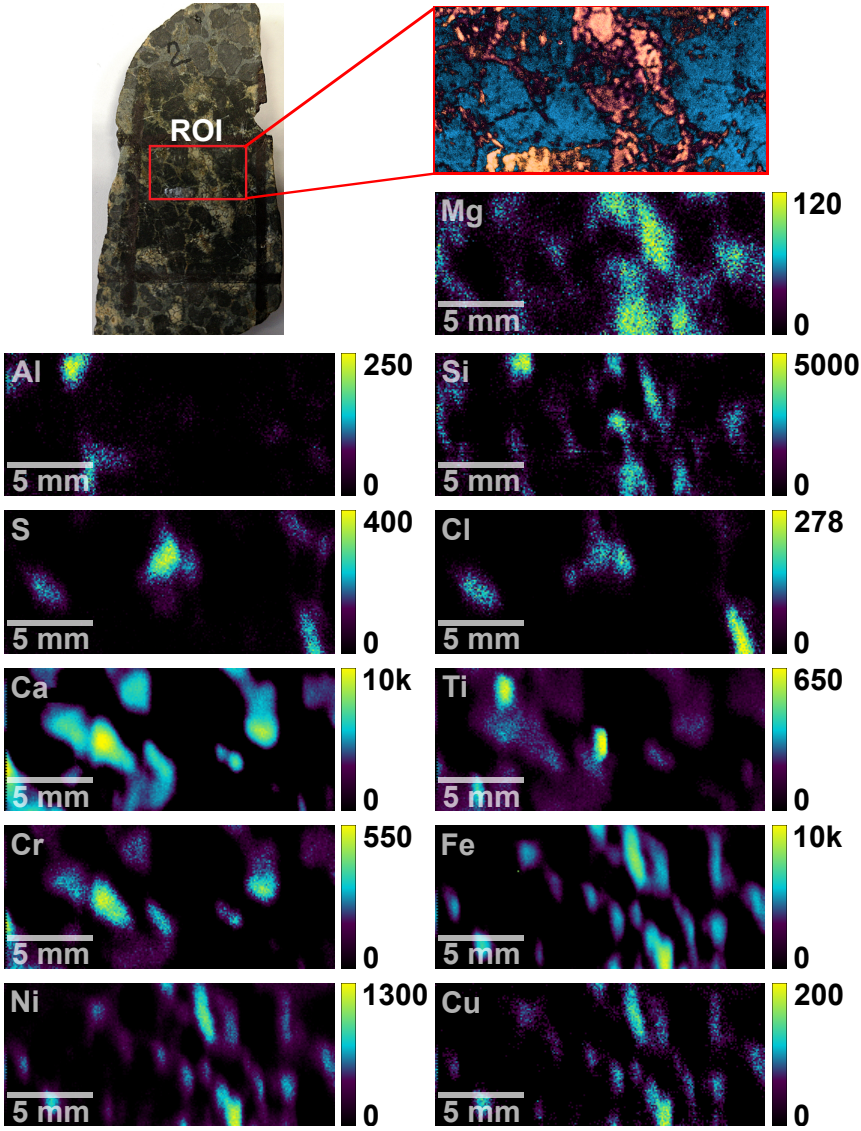

Figure 4.17: Reconstruction of elemental maps for the peridotite sample.

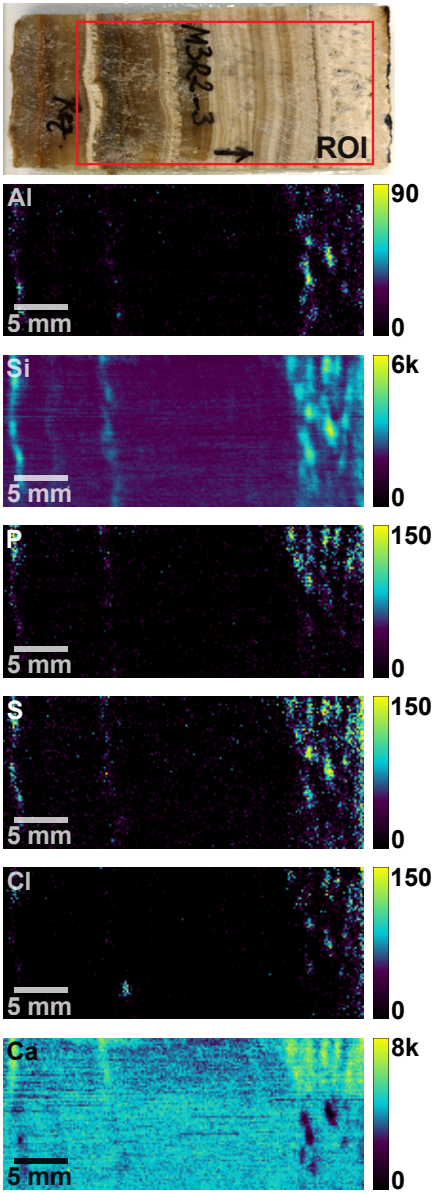

Figure 4.18: Reconstruction of elemental maps for stalactite sample with inventory number M3R2-3.

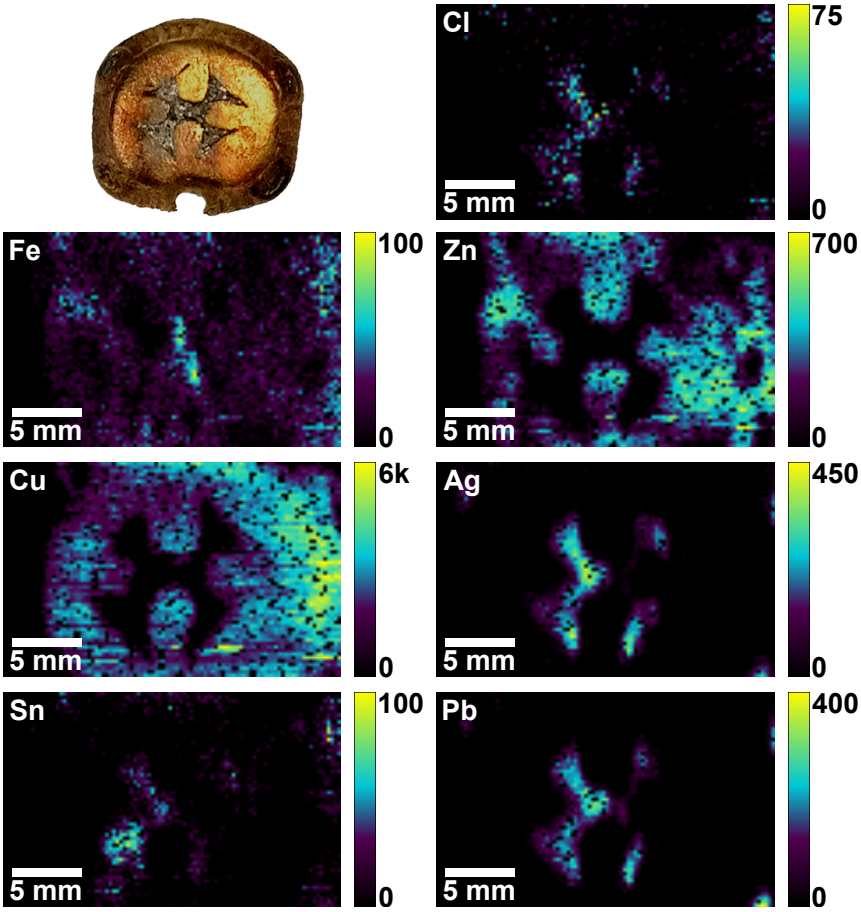

Figure 4.19: Reconstruction of elemental maps for the belt ornament with inventory number INV41236.

Chapter 5

Conclusions and Perspectives

This work addressed three applications of radiation beams in air: 2D/3D elemental mapping using XRF, pulsed irradiation of biological samples with a proton beam in air, and quantitative/qualitative elemental analysis and 2D mapping of chemical elements using PIXE.

The XRF-based mapping system provided high-resolution images for high scanning speeds on unprepared geological samples. The method combined the capabilities of two commercial scanners (ITRAX and M4Tornado) into a single device by scanning the sample in three dimensions. The scanned area was three times larger than that of the standard method, improving statistics when used for 1D representation. In 2D and 3D visualization modes, rock conglomerates could be measured with high precision due to the small pixel size of 0.5 x 0.5 mm^2. Future improvements for this system include redesigning the motion system for high stability and the ability to scan larger, irregularly shaped objects. Additionally, the use of 2-3 detectors will improve statistics and reduce total scan time, while focusing optics like polycapillary lenses can enhance system resolution.

Pulsed Proton Irradiation of Biological Samples: The pulsed proton irradiation system was repeatedly tested to ensure dose repeatability between experiments. Measurements with the Markus camera showed ab-

sorbed doses at various distances from the accelerator window to be in line with Geant4 simulations. The duration of the proton pulses was accurately measured with the IBA reaction chamber's goniometer, with pulse duration differences of less than 0.5% compared to the set value in the signal generator. Irradiating fibroblast cells at different dose rates resulted in survival rates comparable to similar published results.

The PIXE-based quantitative and qualitative elemental analysis proved to be effective, providing precise results. Improvements in determining elemental concentrations were achieved by redesigning the helium purge system based on COMSOL simulations and by enhancing the solid angle of the detector, using a 3D-printed support that placed the detector just 1.5 cm from the sample. The lifespan of the silicon nitride windows was improved through a new fixing method involving the release of mechanical and thermal stress by applying a small amount of epoxy resin to seal the edges.

Elemental mapping using PIXE proved to be an efficient method for analyzing non-homogeneous samples. The obtained maps were reconstructed at good resolutions with acceptable clarity, sufficient for identifying the shapes of structures within the samples. Correcting for the proton beam intensity variation using a witness material was an effective method for achieving uniform maps.

For the XRF elemental mapping system, future plans include redesigning the entire motion system for improved stability, enabling the scanning of larger irregularly shaped samples with 5-6 degrees of freedom. Using 2-3 detectors will enhance statistics and reduce scan times. Incorporating a laser system to measure surface profiles for irregular objects will allow for precise trajectory planning. Additionally, using polycapillary lenses to focus the X-ray beam to 1-5 µm will improve system resolution.

For the pulsed proton irradiation system, there is a need to separate the irradiation of biological samples from elemental analysis by building a dedicated line for biological sample irradiation. Currently, transitioning from biological sample irradiation to elemental analysis mode requires substantial modifications, including realigning components, which is not straightforward and time-consuming.

Eliminating the effects of beam variation without using numerical uniformization methods involves implementing a fast beam scanning system, similar to those used in electron microscopy, on both the X and Y axes. This will substantially reduce scan times and increase map resolution. Building an identical deflector on the X-axis and developing a dedicated pulsing unit for beam scanning will be necessary. Electronic components for beam scanning and synchronization with data acquisition need to be constructed.

In conclusion, the research conducted in this work has advanced the capabilities of radiation-based analytical methods and contributed to the understanding and improvement of various systems used for elemental analysis, mapping, and biological sample irradiation. Future developments will continue to enhance these systems, making them even more powerful tools for scientific research and applications.